Polymer 51 (2010) 5122–5134

Contents lists available at ScienceDirect

Polymer

journal homepage: www.elsevier.com/locate/polymer

Shielding effects in polymer–polymer reactions, 3. Z-RAFT star polymerization under various solvent conditions

Markus G. Fröhlich [a], Michael M. Nardai [a], Nadja Förster [b], Philipp Vana [b], Gerhard Zifferer [a,*]

[a] Department of Physical Chemistry, University of Vienna, Währinger Str. 42, A–1090 Wien, Austria
[b] Institute of Physical Chemistry, Georg-August-University Göttingen, Tammannstraße 6, D–37077 Göttingen, Germany

ARTICLE INFO

Article history:
Received 12 July 2010
Received in revised form
11 August 2010
Accepted 25 August 2010
Available online 28 September 2010

Keywords:
RAFT polymerization
Dissipative particle dynamics
Monte carlo simulation

ABSTRACT

Shielding effects of the surrounding arms and the chain on the encounter probability of reactive sites taking part in the Z-RAFT star polymerization are investigated (a) by use of lattice based Monte Carlo simulations in combination with exact enumeration techniques and (b) by direct simulation applying an off-lattice coarse-grained molecular dynamics method (dissipative particle dynamics, DPD). Making use of the former method the chain-length dependence of the shielding factors is discussed for a broad range of thermodynamic conditions and compared to DPD results for the athermal (good solvent) and theta (bad solvent) case, i.e., for the limiting solvent qualities evaluated. In addition, changes of the size and shape of the reaction partners on approach and penetration are discussed in some detail. The results of both simulation methods fairly well coincide and reveal that shielding is smaller and chain-length dependence less pronounced under theta conditions as compared to good solvent conditions. Experimentally determined polydispersities of polystyrene generated by Z-RAFT star polymerizations in the poor solvent cyclohexane were found to be smaller than with the good solvent toluene, which is in full accordance to the theoretical predictions.

1. Introduction

Properties of star-branched polymers, i.e., macromolecules with one distinct central branching point and several polymeric arms are rather distinct from properties of linear chains of the same molecular weight. Several features of polymeric material are largely influenced by the topology of the underlying polymer chains, for example, zero-shear viscosity (for constant molecular mass) is the lower the larger is the number of arms [1]. Because of their interesting characteristics star-branched polymers are attracting attention since years and a lot of effort was put into the investigation of properties of stars as well as into the development of new methods for their synthesis. A most promising method (among others, usually anionic techniques [2–4]) for the synthesis of well defined star-branched polymers with narrowly distributed and predefined molecular weights is the so called reversible addition-fragmentation chain transfer polymerization (RAFT) [5–7] which is based on controlled (living) radical polymerization [8]. Due to the reversible transfer process, the active, i.e., propagating species (polymer radicals) are in equilibrium with the dormant polymeric RAFT compounds and thus all chains have an equal growing probability. In order to produce star-branched polymers in a 'core-first' fashion, RAFT agents, for example thiocarbonylthio-compounds [S = C(Z)SR] (with S being sulfur, C carbon, and Z and R the stabilizing and leaving group, respectively, see also Scheme 1 and Scheme 2a) may be coupled to form a multifunctional mediating agent. By usage of a judiciously designed multifunctional stabilizing group Z – constituting the center of the (dormant) star – a polymerization is induced in which the growing radical R is located at the end of a linear chain (i.e., the arm, propagating species) and the equilibrating reaction occurs at a small (central) unit. As a matter of fact, the controlling reaction of this strategy, which is referred to as Z-RAFT star polymerization [9–12], may clearly be shielded by the surrounding polymer segments. In former studies [13,14] we investigated this shielding effect for athermal (i.e., good) solvents as a function of functionality (i.e., the number of arms), chain stiffness and the size of the core segment by use of a combined lattice based Monte Carlo (MC) and exact enumeration (EE) technique. In the present work the influence of the thermodynamic solvent condition on the shielding effect is investigated on the example of the Z-RAFT star polymerization of four-arm stars. In addition to the (static) MC simulation a most promising (dynamic) off-lattice technique – namely dissipative particle dynamics (DPD) [15,16] – is used in order to simulate the dynamic behavior of the involved molecules.

First, parameters indicating theta conditions are introduced. Second, shielding factors are investigated by MC + EE with respect

* Corresponding author. Tel.: +43 1 4277 52436; fax: +43 1 4277 9524.
E-mail address: gerhard.zifferer@univie.ac.at (G. Zifferer).

0032-3861/$ – see front matter © 2010 Elsevier Ltd. All rights reserved.
doi:10.1016/j.polymer.2010.08.054

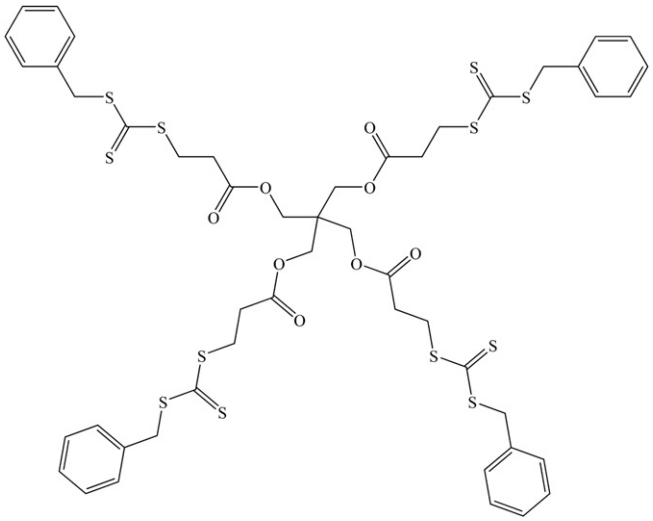

Scheme 1. Star-shaped Z-RAFT agent **1** used in this study.

to their dependence on chain lengths for a broad range of solvent qualities ranging from athermal to theta conditions. Third, these results are compared to DPD calculations for the limiting cases, i.e., for the athermal and the theta solvent. Forth, properties which characterize the size and shape of the molecules are calculated as well as their differential changes while the molecules approach, in order to compare the 'pseudo-dynamic' interpretation of the statically obtained MC data with the 'real' dynamics of DPD data. Finally, experimental results for the Z-RAFT star polymerization of styrene in the poor solvent cyclohexane are given and compared to experiments in the good solvent toluene.

2. Computational and experimental method

2.1. Monte Carlo and exact enumeration

In order to reduce the time-consuming evaluation of contact probabilities within compatible star/chain pair configurations to a counting problem non-intersecting star-branched polymers with $F = 4$ arms as well as linear chains are embedded in a simple 5-way cubic lattice. To mimic the central step of Z-RAFT star polymerization the number of bonds n of the linear chain is equal to the number of bonds within the detachable arms of the star (which are attached to a common central bead) ranging from $n = 8$ to 256 as described in [13]. Thus the number of segments m per arm (chain) amounts to $m = n + 1$ and the total number of segments reads as $N_1 = m$ for linear chains and $N_2 = 1 + F \cdot m$ in case of star-branched molecules.

The procedure for the production of non-athermal chains (which is similar to the method for athermal conditions, see [13] for details) is shortly explained here for clarity and convenience of the reader: Two independent pools each consisting of 300 stars and chains, respectively, are produced by use of the PIVOT algorithm [17,18]. Starting from entirely elongated molecules in case of athermal conditions and athermal stars and chains otherwise these initial configurations are subjected to about 25 relaxation steps per segment. For each relaxation trial one segment is randomly selected and one randomly chosen symmetry operation (out of the 47 possibilities excluding identity for this lattice) is applied to all segments of the smaller part of the molecule. The acceptance of the new configuration is controlled by the well known Metropolis–Rosenbluth algorithm [19], i.e., the new configuration is accepted if its energy is smaller than or equal to that of the old one or otherwise with a probability $\exp(-\varphi \cdot \Delta c)$, $\varphi = \varepsilon/k_B T$ being the interaction parameter measuring the energy ε of one contact (i.e., two non-bonded segments in a distance of 1 lattice unit) in multiples of $k_B T$ and Δc being the difference of the total number of new and old *intra*molecular contacts. In case of athermal systems the interaction parameter $\varphi = 0$, thus each overlap free configuration is accepted.

For the exact enumeration of pair configurations, according to a method described in [13,20], an ensemble of $24 \cdot 10^6$ pairs of interacting molecules is determined as follows: Both linear and star-branched chains are randomly selected from the respective pool and their centers of gravity – rounded to integer numbers – are forced to coincide at the origin of the coordinate system. In a second step all segment–segment (overlap) vectors as well as all nearest neighbor

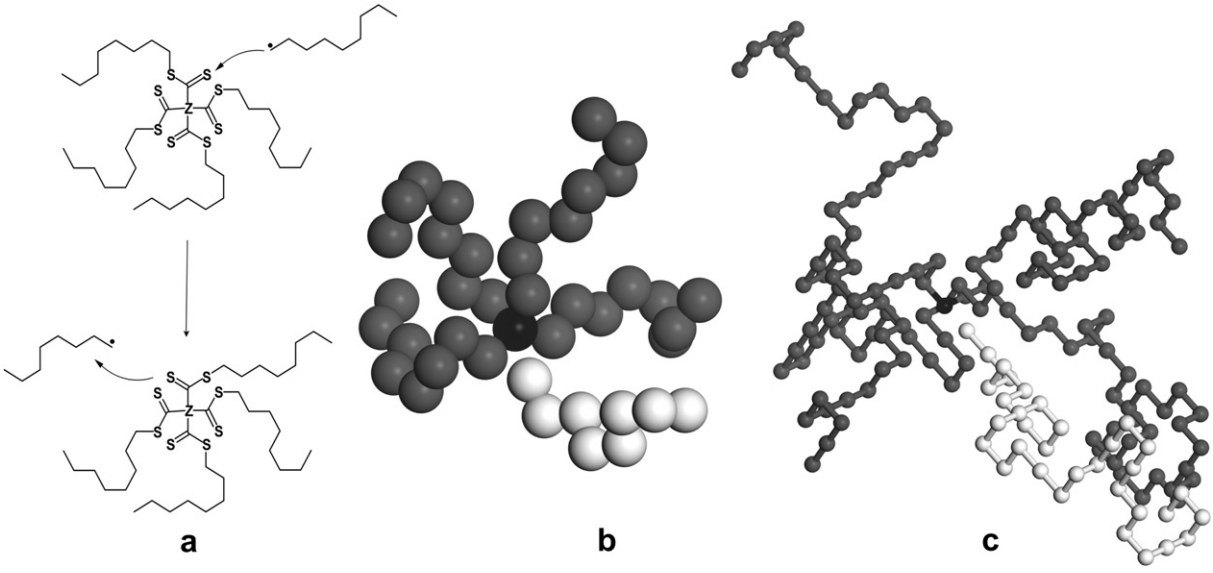

Scheme 2. Central reaction step of Z-RAFT four-arm star polymerization (a) and schematic representations of allowed configurations with both the center of the star (black) and the end of the linear chain (white) in contact: DPD (b), MC + EE (c).

vectors (vectors from segments of the first chain to nearest neighbor positions of segments of the second one) are enumerated, the former resulting in the number of forbidden pair configurations M_f and the latter – after elimination of nearest neighbor vectors which coincide with overlap vectors – in the number of allowed pair configurations $M_{a,k}$ ($k \geq 1$) with at least one contact (whereas the multiplicity k of a given vector represents the number of *inter*molecular contacts between both chains for a certain distance r between their centers of mass characterized by the length of this vector), respectively. The number of allowed pair configurations without any contact is given by $M_{a,0} = M_t - M_f - \sum M_{a,k}\,(k \geq 1)$, as the number of all accepted pair configurations (regardless of their number of contacts) is simply the difference between the total number of possible configurations M_t with distance r (easily countable in a lattice) and the forbidden ones. It should be noticed that all these M values are functions of the separation r which actually are sampled in form of histograms with bin-width $\Delta r = 1$. The calculation of M_t and $M_{a,k}\,(k \geq 0)$ is necessary (1) to arrive at the statistical weight of the pair configuration, expressed by the intermolecular Boltzmann factor and (2) allows the evaluation of quantities depending on separation distance r between the two centers of gravity, e.g., the pair distribution function and size and shape factors (see Section 3. 'Calculated properties' below).

Due to the chosen dynamic production algorithm consecutively generated chains are correlated. Hence in order to avoid pair configurations consisting of biased molecules each selected configuration is additionally subjected to 10 relaxation steps per segment – as described above – before being restored into the respective pool. For the actual pool size of 300 independent stars or linear chains, respectively, the average probability for selecting a certain pair ($1/300 \cdot 1/300 \approx 10^{-5}$) is rather small. Thus, statistical independence of all pair configurations is guaranteed as in total a large number of relaxation steps is performed between two comparisons of 'the same' pair. The standard deviation of data is smaller than 0.2%.

2.2. Dissipative particle dynamics (DPD)

In the DPD simulation [15,16] the atomistic representations of the polymer molecules (four-arm stars and linear chains) are replaced by off-lattice (coarse-grained) equivalent chains by combining both monomers as well as solvent molecules to beads within a three-dimensional simulation box with periodic boundary conditions in all directions. In order to mimic the excluded volume effect polymer as well as solvent beads are repulsive for each other. The underlying interaction potential is chosen to be relatively weak and without any attractive term, in contrast to a Lennard Jones type potential. Also it is quite short ranged by definition, with a cutoff radius r_c nearly as short as the typical bond length of a DPD chain. An implementation of the latter one is achieved by linking successive beads within polymer chains with additional spring potentials.

The system is relaxed by molecular dynamics solving Newton's equations of motion, which is performed by use of a slightly modified Verlet velocity algorithm. Particles propagate under the influence of short ranged *conservative* forces – i.e., repulsion of non-bonded beads and a proper balance of repulsion and attraction between bonded segments, as mentioned above – and *dissipative* forces due to friction between particles, the latter representing the thermostat in conjunction with proper *random* forces. The explicit treatment of solvent and the preservation of Galilean invariance by the DPD thermostat give rise to momentum transport within the fluid and thus allow for correct hydrodynamic interaction.

Polymer chains evolve in a bath of single solvent beads, in which different thermodynamic conditions are accessible by a variation of the repulsion parameter a_{ij} measuring the strength of the repulsive force between different types of beads i and j in units of k_BT/r_c [16,21]. With index $p(s)$ designing a polymer (solvent) bead, the case $a_{ps} = a$ (with $a_{pp} = a_{ss} = a = 25$) refers to athermal conditions while $a_{ps} > (<)\ a$ represents an endothermal (exothermal) solution. Ideal scaling of mean square dimensions with respect to chain lengths is found at $a_{ps} \approx 27.2$ thus defining theta conditions for infinite chain lengths [21]. Details of the simulation procedure are not repeated here but can be found in [21] as well as the simulation parameters chosen. It should be noticed that all distances are given in multiples of r_c.

As a matter of fact the dynamic approach is much more time-consuming compared to MC restricting the accessible arm length to $m \leq 32$. Depending on the radii of gyration of both the star-branched chain and the linear chain the edge length of the simulation box ranges from 10 to 20, thus assuring that neither the linear chain nor the star 'feels' its periodic image and that interaction free distances are accessible to the solutes allowing for convergence of the pair distribution function to a value of 1 (unrestricted compatibility).

The accuracy of the data is less than in case of MC + EE but the standard deviation of distance dependant data doesn't exceed 3–4% in the worst case (data at small distances).

2.3. Experimental procedure

2.3.1. RAFT agent synthesis

The tetrafunctional RAFT agent pentaerythritol-tetrakis-(3-(S-benzyl-trithiocarbonyl)-propanoate) **1** (see Scheme 1) was synthesized according to the procedures shown by us [22] and others [23].

2.3.2. Solution polymerization

Styrene (≥99.0%, Fluka, purified by passing through a column filled with inhibitor remover), cyclohexane and toluene (both purchased from Aldrich) were degassed via three freeze-pump-thaw cycles, transferred along with RAFT agent **1** and initiator di(2-ethylhexyl)peroxydicarbonate (purchased from AKZO Nobel) into an argon-filled glove box (oxygen content below 2 ppm), where stock solutions of 3 mL monomer, 9 mL solvent (toluene or cyclohexane), initiator and RAFT agent were prepared. Ten samples of each stock solution were filled into individual glass vials and sealed with Teflon/rubber lids. The vials were subsequently inserted into a block heater, thermostated at 47 ± 0.1 °C. The samples were removed after preset time intervals and cooling the solution in an ice bath stopped the reaction. Monomer-to-polymer conversions were determined gravimetrically.

2.3.3. Polymer characterization

Molecular weight distributions were determined by size-exclusion chromatography (SEC) using a JASCO AS-2055-plus auto-sampler, a Waters 515 HPLC pump, three PSS-SDV columns with nominal 5 μm particle size and pore sizes of 10^5, 10^3 and 10^2 Å, a Waters 2410 refractive index detector, a Viskotek VE3210 UV/VIS-detector, and THF at 35 °C as the eluent at a flow rate of 1.0 mL min^{-1}. The SEC set-up was calibrated with linear polystyrene standards of narrow polydispersity (M_p = 410 to 2 000 000 g mol^{-1}) from Polymer Standards Service.

3. Calculated properties

3.1. Pair distribution functions and excluded volume

Within the MC + EE approach the pair distribution function $g(r)$, which represents the probability $g(r) \cdot \Delta r$ of finding two compatible (non-intersecting) chains at a certain separation distance r, e.g., the distance between their centers of gravity, for athermal conditions

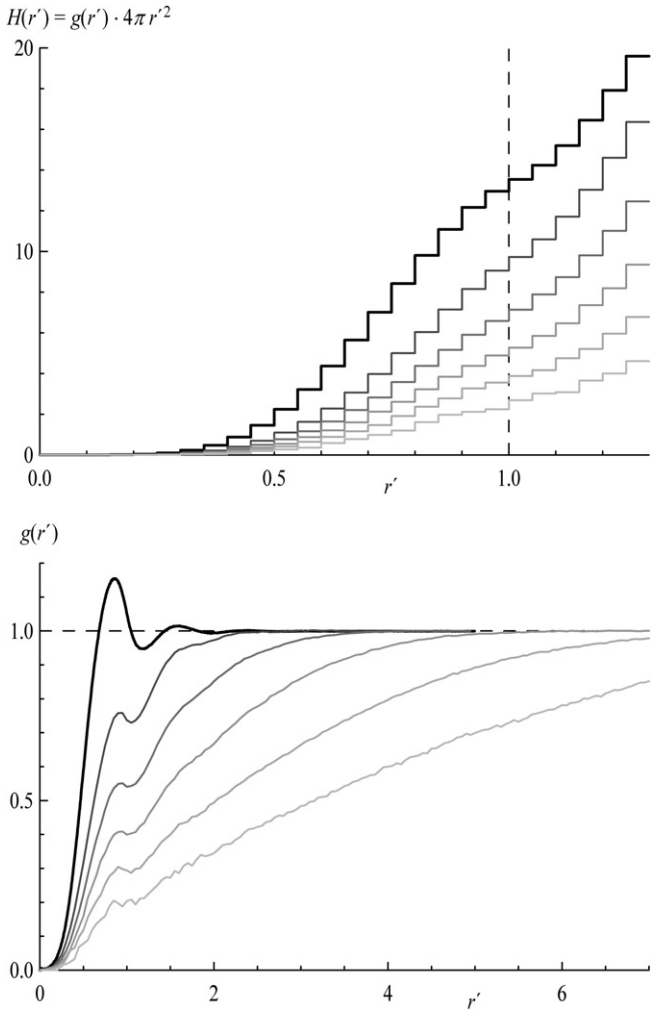

Fig. 1. DPD frequency plot (top) and corresponding center-end distribution (bottom) as functions of distances between the center of the star and the ends of the linear chain for all investigated chain lengths $m = 2$–32 (represented by grayscales from dark to light). The black line depicts the unshielded monomer–monomer (reference) situation.

simply equals the fraction of accepted pairs being within the interval $[r, r + \Delta r]$, i.e., $M_a/M_t = (M_t - M_f)/M_t$. For non-athermal conditions the probability of a certain pair configuration k is given by its (intermolecular) Boltzmann factor $\exp(-E(r)/k_BT)$ which is zero in case of an overlap between the chains and $\exp(-\varphi \cdot C_k)$ for accepted configurations with C_k being the number of intermolecular contacts and φ again being the energy parameter, characterizing the solvent quality, as defined in Section 2.1. Thus, quite generally,

$$g(r) = \left\langle e^{-E(r)/k_BT} \right\rangle \tag{1}$$

which degenerates into the fraction of accepted chains in case of athermal conditions (Boltzmann factor either zero or one) as stated above. Anyway, all required values may be deduced from the M values defined in Section 2.1.

In case of DPD calculations $g(r)$ is obtained from the frequency plot $H(r)$ which represents the time average of pair configurations exhibiting separation within interval $[r, r + \Delta r]$ normalized so that

$$g(r) = \frac{H(r)}{4\pi r^2 \Delta r} \tag{2}$$

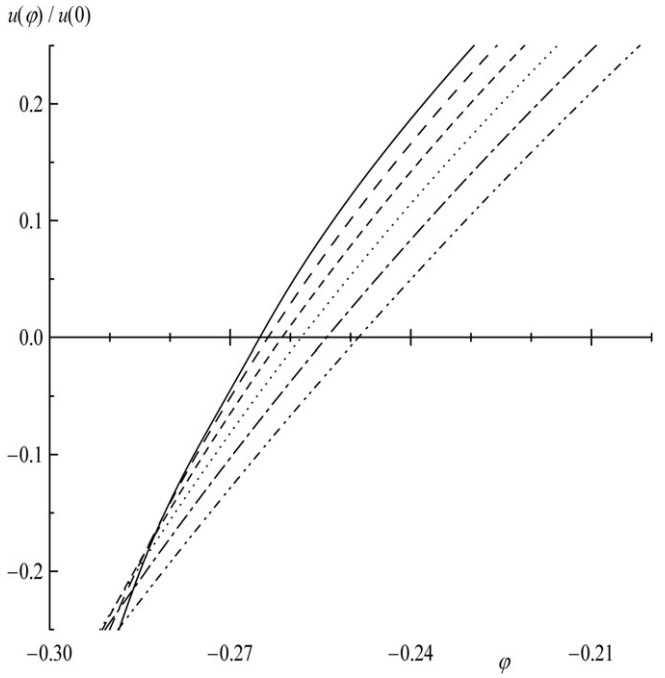

Fig. 2. Reduced intermolecular excluded volume vs. MC interaction parameter for chain/arm lengths of $m = 257$ (full line), 129 (long-dashed line), 65 (short-dashed line), 33 (dotted line), 17 (long-dash dotted line) and 9 (short-dash dotted line) segments.

converges to 1 for large values of r. It should be noted that $H(r)$ is equivalent to M_a while the volume of the spherical shell spanned by the width of the histogram bins takes the role of M_t. However, no Boltzmann factors appear in the dynamic approach for any thermodynamic conditions as the position of the chains 'naturally' evolve as a function of time as well as penetration of chains, contact building and accompanying deformations resulting in changes of size and shape.

For MC + EE as well as DPD the pair distribution function is related to the excluded volume by

$$u = \sum [1 - g(r)] \cdot 4\pi r^2 \Delta r \tag{3}$$

It should be mentioned that the distance r usually denotes the separation between the two centers of gravity of both molecules, however, especially concerning the central step of Z-RAFT star polymerization some properties are additionally evaluated as function of the distance r' between the two active sites (i.e., the center of the star and the end of the linear chain).

3.2. Shielding factors K

Following the concept described in [24] the shielding factor $K = k/k_0$ – being the rate constant k of a bimolecular polymer–polymer reaction divided by the rate constant k_0 characterizing the same reaction but the reactive sites not located at polymer chains – is quite generally given by the probability of contact formation between two specified segments i and j (the former located on the one and the latter on the other chain) and ranges from 0 for perfect shielding to 1 for the unshielded situation.

Within the MC + EE approach for athermal conditions K values, K_{ij}, of contact formation between segment i of the first and segment j of the second chain are calculated by

$$K_{ij} = M_{ij}/(M \cdot z) \tag{4}$$

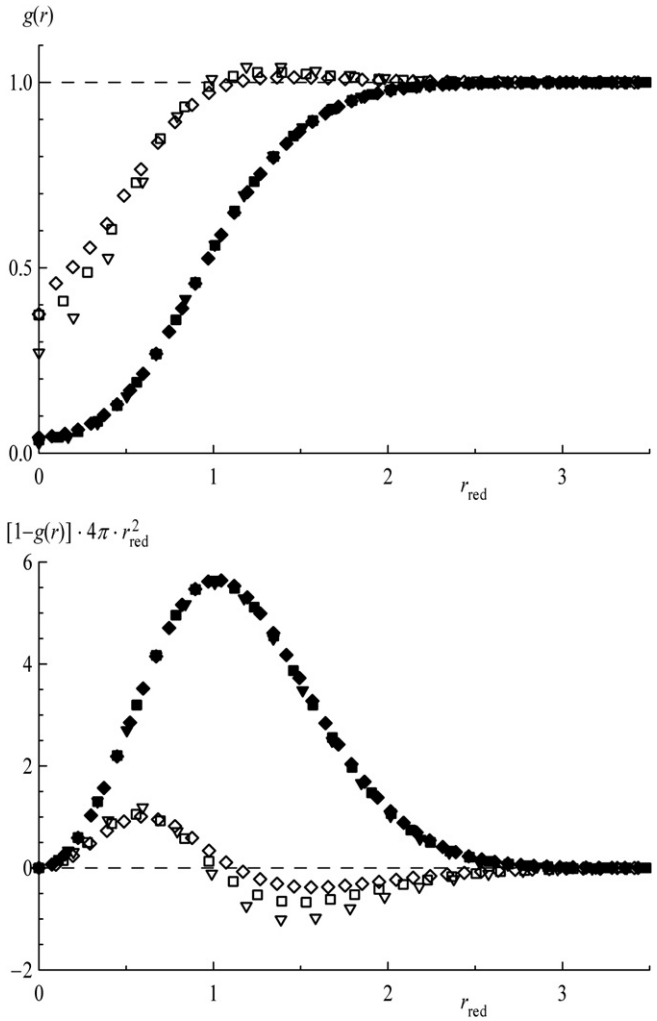

Fig. 3. MC pair distribution function (top) and integrand of the intermolecular excluded volume (bottom) as function of reduced separation distance between the centers of gravity of both molecules. Data for athermal (theta) conditions are shown in full (open) symbols for chain/arm lengths of $m = 33$ (inverted triangles), 65 (squares), and 129 (diamonds).

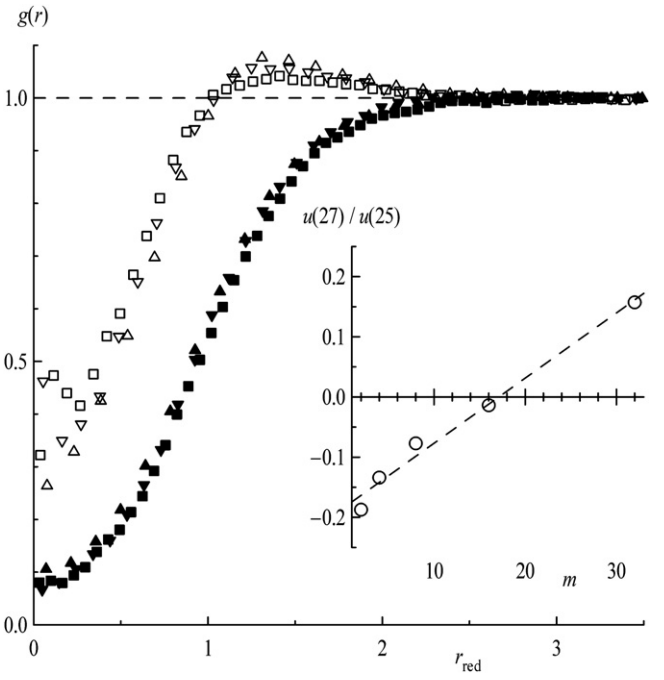

Fig. 4. DPD pair distribution function versus reduced separation distance r_{red} for chain lengths of $m = 4$ (triangles), 8 (inverted triangles) and 16 (squares) beads. Data for athermal (theta) conditions are shown in full (open) symbols. The inset shows the reduced intramolecular excluded volume at $a_{ps} = 27$ as a function of chain length.

where M_{ij} is the number of accepted (overlap free) configurations with segments i and j in contact (i.e., in a distance of one lattice unit), M is the total number of pair configurations evaluated, and z the maximum number of available free lattice sites for contact formation. As already discussed above, for non-athermal conditions the probability of an accepted pair configuration k is given by its Boltzmann factor $\exp(-\varphi \cdot C_k)$ based on the number of intermolecular contacts C_k. Thus, M_{ij} in Eq. (4) has to be replaced by the sum of Boltzmann factors over all accepted configurations M_a with (at least) segments i and j in contact and all required values again may be deduced from the M values defined in Section 2.1.

In the actual case the reactive sites are located at the central bead (c) of the star-branched molecule and the terminal, i.e., end bead (e) of the linear chain (representing the reactive sites in Z-RAFT star polymerization, as described above, see Scheme 2). For comparison two further cases are treated, i.e., contact of the terminal beads of the linear chain with terminal beads of the star (end segments of arms) and with beads located in the middle of arms of the star (MC + EE only).

In a dynamic simulation, K_{ce} may be calculated directly on basis of the original definition by building the ratio:

$$K_{ce} = \frac{\sum\limits_{0<r'<1} H(r')}{\sum\limits_{0<r'<1} \tilde{H}(r')} \tag{5}$$

with $H(r')$ being the frequency of distances between the center of the star-branched molecule and the end of the linear chain (shielded situation), and $\tilde{H}(r')$ denoting the frequency of distances between two single beads (unshielded reference situation). By applying the idea of contact formations to an off-lattice model with soft interaction forces, a threshold distance corresponding to the strict definition of neighboring segments is needed. Conveniently, in the DPD simulation each distance smaller than the cutoff radius r_c, i.e., $r' < 1$, is defined as a contact. The procedure is demonstrated for athermal conditions in Fig. 1.

It should be noted that shielding factors K defined as ratios of equilibrium contact probabilities correspond to relative rate constants as defined above primarily in case of chemically controlled reactions which are slow enough to occur from equilibrium pair configurations. In case of (center of mass) diffusion controlled reactions, the chain length dependence of (relative) reaction rates should, on the other hand, be dominated by that of the diffusion coefficients. However, as outlined in detail in Ref. [24], the concept of equilibrium pair configurations also holds true if segmental diffusion of the reactive groups within a contact pair is the rate controlling process. This is for instance the case for bimolecular termination reactions in radical polymerization, at least for the limit of long chains, as indicated by the magnitude of relaxation times of molecular motions [25] and experiments. As radical addition to RAFT-groups generally is slower than termination, the concept of equilibrium pair configurations almost certainly applies to Z-RAFT star polymerization, as well.

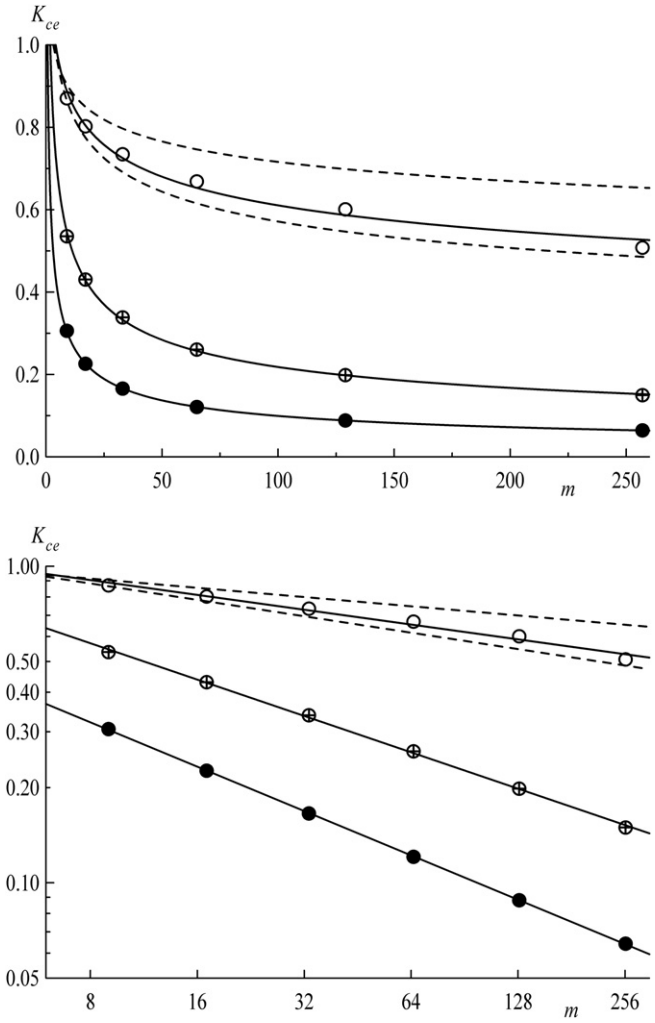

Fig. 5. Normal plot (top) and log–log plot (bottom) of shielding factors K_{ce} of contact formation between the center of a four-arm star and the end of a linear chain as a function of chain/arm length m obtained by Monte Carlo simulation for different thermodynamic solvent qualities: $\varphi = 0$ (full circles), $\varphi = -0.15$ (crossed circles) and $\varphi = -0.261$ (open circles).

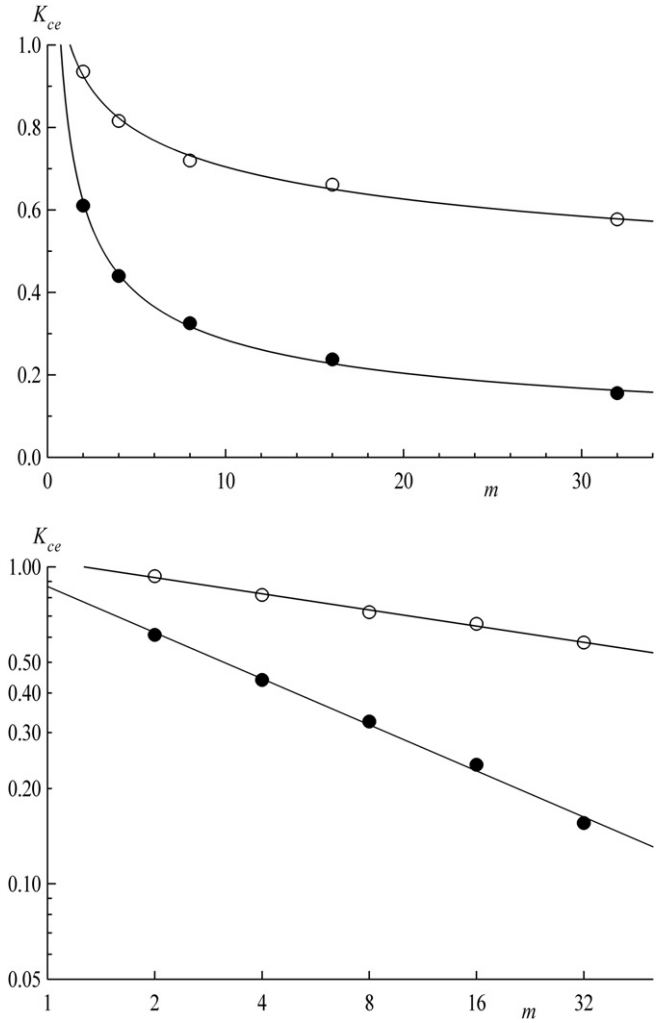

Fig. 6. Shielding factors K_{ce} vs. chain length m obtained by dissipative particle dynamics method for athermal conditions, $a_{ps} = 25$ (full circles), and theta conditions, $a_{ps} = 27$ (open circles).

3.3. Size and shape

In order to characterize the average size of single molecules the mean square radius of gyration $\langle s^2 \rangle$ – defined as the average of the squared distances of segments (beads) to their common center of mass – is evaluated. Based on the principal components L_i^2 of the square radius of gyration $s^2 = L_1^2 + L_2^2 + L_3^2$ of individual configurations taken along the principal axes of inertia – representing the chain as an equivalent ellipsoid [26,27] – the instantaneous shape of a molecule may be described by an asphericity parameter [28,29],

$$\delta^* = \frac{\left(3L_1^2 - s^2\right)^2 + \left(3L_2^2 - s^2\right)^2 + \left(3L_3^2 - s^2\right)^2}{6\left(L_1^2 + L_2^2 + L_3^2\right)^2} \tag{6}$$

which reaches values $\delta^* = 0$ for perfect spheres, $\delta^* = 1/4$ for circular disks and $\delta^* = 1$ for rod-like structures. For detailed information on these quantities see Ref. [30].

To represent the situation at infinite separation of both molecules averages $\langle x \rangle$ are obtained as follows: In case of lattice MC simulations ensemble averages over all configurations are taken into account as any pair configuration is allowed due to the absence of overlaps. Comparably, in case of DPD simulation time averages are obtained by sampling only unperturbated pair configurations (i.e., r is large enough to ensure $g(r) = 1$). Averages $x(r)$ taken over chains and stars being part of accepted pairs (i.e., overlap free configurations in case of MC; DPD configurations are overlap free a priori) within interval $[r, r + \Delta r]$ directly yield characteristic chain-data as function of separation allowing for a dynamic picture that reflects the differential changes of the molecular properties when both polymers approach. Clearly, by use of MC + EE this picture is only a pseudodynamic one as the entire information is statically obtained from all accepted and properly weighted pair configurations subsequently interpreting the results dynamically by splitting them into contributions referring to actual distances, e.g., between their centers of mass [31].

4. Results and discussion

4.1. Solvent quality

As we are interested in the influence of solvent quality on shielding effects definition and controlling of thermodynamic

conditions should be discussed first. Especially, the determination of a proper interaction parameter φ_Θ which is characteristic for theta solvent conditions is, to some extent, a challenge for both the lattice MC and the DPD calculations. Numerical values usually are obtained by use of an intramolecular criterion ($\langle s^2\rangle \sim N-1$), which leads to an (average) theta parameter valid for *all* chain lengths. As such calculations refer to single and thus to rather long chains such an estimate of φ_Θ may be regarded as a long chain limit. Alternatively, theta conditions may be based on the intermolecular criterion of a vanishing excluded volume which has to be calculated for any desired chain length. Actually, φ_Θ calculated in this latter way is showing a certain chain-length dependence [20] slowly converging to the long chain limit introduced above.

For linear chains embedded in the 5-way cubic lattice on the basis of the intramolecular criterion an energy parameter $\varphi_\Theta \approx -0.27$ is expected within the limits of $N\to\infty$ [32]; however, for short chains (with $n \approx 30$–40) a value of $\varphi_\Theta \approx -0.255$ is more adequate for making the second osmotic virial coefficient vanish [24].

In the present investigation we are concerned with the pair distribution function $g(r)$ and the excluded volume $u = \sum[1-g(r)]\cdot 4\pi r^2\Delta r$ between a star-branched chain and a linear one: In Fig. 2 the reduced excluded volume – i.e., the ratio of the excluded

Table 1
Prefactors A and exponents ε of power laws $K = A\cdot m^\varepsilon$ obtained by Monte Carlo simulations for interaction parameters φ indicated.

φ	center end		middle end		end end	
	A	ε	A	ε	A	ε
0	0.846	−0.465	0.843	−0.285	0.796	−0.163
−0.015	0.886	−0.461	0.873	−0.283	0.818	−0.162
−0.030	0.924	−0.456	0.902	−0.281	0.841	−0.161
−0.045	0.967	−0.451	0.933	−0.278	0.864	−0.160
−0.060	1.009	−0.445	0.966	−0.275	0.888	−0.158
−0.075	1.051	−0.437	0.999	−0.271	0.913	−0.156
−0.090	1.097	−0.429	1.033	−0.267	0.939	−0.154
−0.105	1.140	−0.419	1.067	−0.262	0.965	−0.151
−0.120	1.184	−0.409	1.104	−0.256	0.993	−0.148
−0.135	1.224	−0.396	1.138	−0.249	1.020	−0.145
−0.150	1.263	−0.381	1.172	−0.241	1.047	−0.140
−0.165	1.296	−0.364	1.204	−0.231	1.075	−0.135
−0.180	1.326	−0.344	1.233	−0.219	1.101	−0.128
−0.195	1.337	−0.319	1.257	−0.205	1.124	−0.119
−0.210	1.336	−0.289	1.272	−0.187	1.144	−0.108
−0.225	1.331	−0.257	1.277	−0.165	1.156	−0.094
−0.240	1.308	−0.218	1.258	−0.135	1.161	−0.077
−0.255	1.263	−0.172	1.213	−0.097	1.147	−0.053
−0.261	1.251	−0.156	1.210	−0.085	1.134	−0.040
−0.270	1.118	−0.097	1.177	−0.058	1.115	−0.021

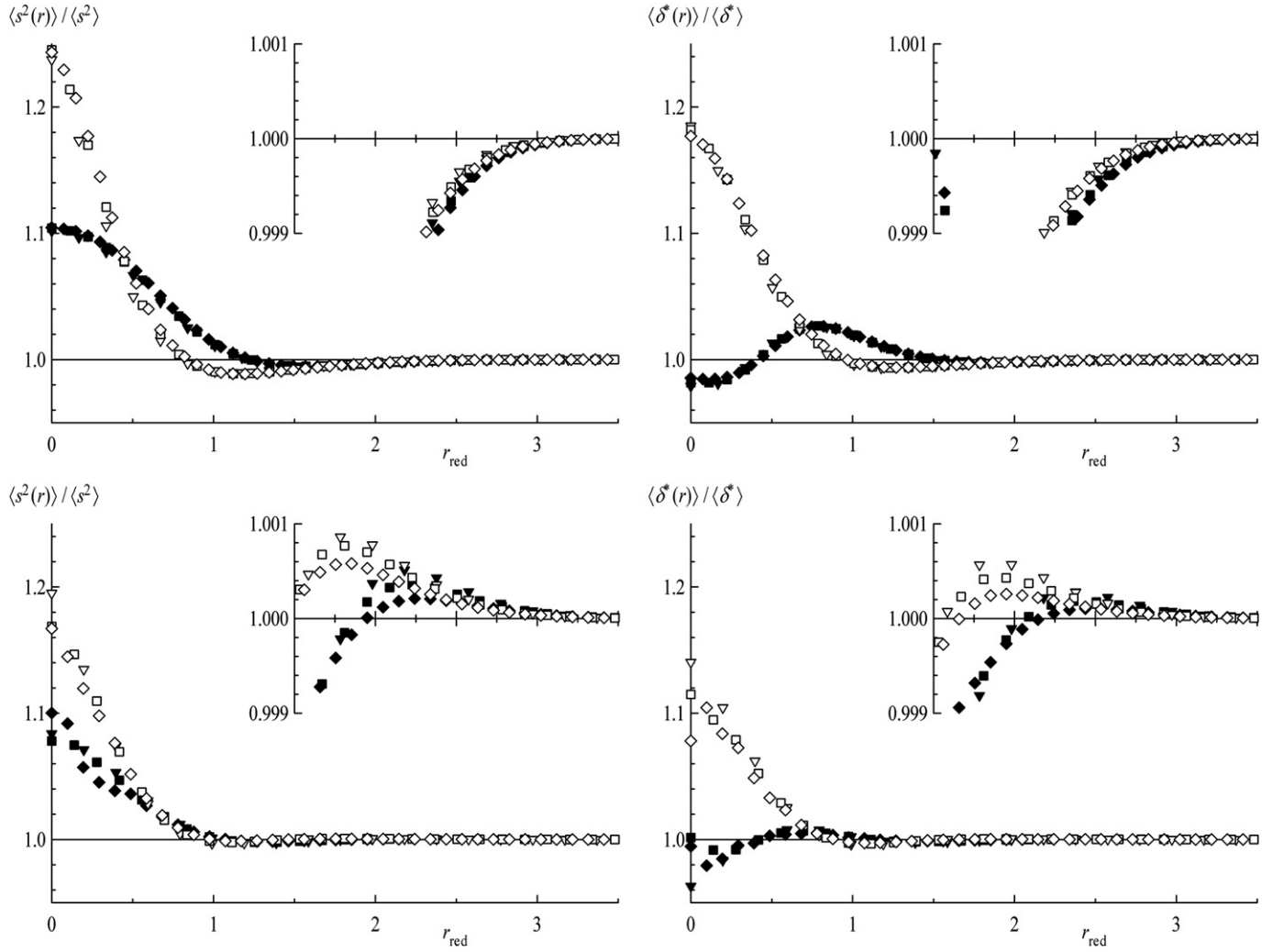

Fig. 7. Relative deviation of the squared radius of gyration (left) and the asphericity parameter (right) from their values at infinite separation as a function of reduced distance r_{red}. Data achieved by MC simulations for stars (full symbols) and linear chains (open symbols) with chain lengths $m = 33$ (inverted triangles), 65 (squares), and 129 (diamonds). Top row refers to athermal, bottom row to theta conditions.

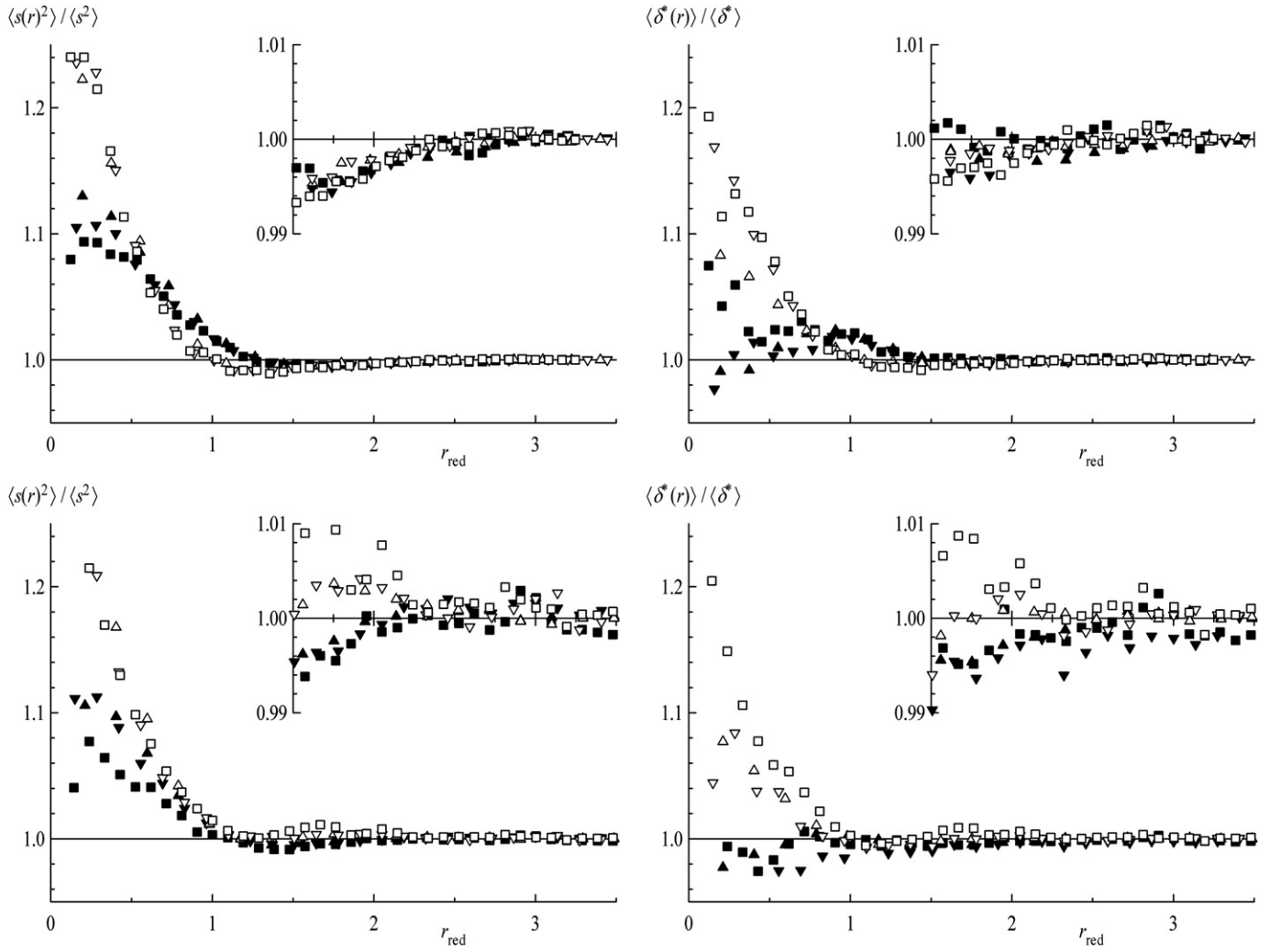

Fig. 8. Size and shape characteristics (analogous to Fig. 7) of athermal (top) and theta conditions (bottom) obtained by DPD simulations for chain lengths $m = 4$ (triangles), 8 (inverted triangles) and 16 (squares) beads. Full symbols refer to the star, open symbols to the linear chain.

(intermolecular) volume for a certain interaction parameter over the excluded volume under athermal conditions − is plotted as a function of φ for all chain lengths investigated by MC simulation in this work. It is clearly seen that φ_Θ actually converges to approximately −0.27 for very long (linear) chains as reported. Considering chain lengths which are used in this work a value $\varphi_\Theta = -0.261$ fulfills the intermolecular criterion best (on average) leading to $u(\varphi)/u(0)$ values between −0.025 and 0.025 for $m = 33$–129 beads per linear chain. As a matter of fact, zero excluded volume is realized by compensation as demonstrated in (the lower part of) Fig. 3 where $g(r)$ as well as the corresponding integrand $[1 - g(r)]\cdot 4\pi r^2$ are shown as functions of the distance between the centers of gravity of both molecules for athermal conditions and for $\varphi = -0.261$; in order to fit data to the same scale reduced separation distances r_{red} are used which are normalized by the root mean square radius of gyration of the (isolated) star.

At zero concentration, starting from infinite separation, $g(r)$ gradually decreases for athermal conditions (full symbols) to roughly $g(0) \approx 0.05$ for all investigated chain lengths. These values are rather large compared to pairs of two four-arm stars, where $g(0)$ exhibits values of one order of magnitude lower but appreciably smaller than $g(0)$ between two linear chains (ca. 0.15) an effect which is clearly caused by the fact that one partner is a linear chain and the other a star. As in case of pure linear and star-branched chains, respectively, $g(r)$ of the mixed system for (near to) theta conditions (open symbols) first becomes larger than 1 before diminishing to about 0.40 at $r_{red} = 0$ for all chain lengths (again between $g(0) \approx 0.5$ of linear chains and $g(0) \approx 0.05$ for four-arm stars [20]).

For athermal conditions $[1 - g(r)]\cdot 4\pi r^2$ is positive throughout (indicating purely repulsive interactions) while for $\varphi = -0.261$ positive contributions at small distances ($r_{red} < 1$) are (more or less) compensated by negative ones at larger distances ($1 < r_{red} < 3$) resulting from attractive interactions. For r_{red} larger than $r_{red} \approx 3.5$ $g(r) = 1$ throughout and the contribution to u accordingly is zero.

For DPD − as already mentioned above − the theta parameter based on the intramolecular criterion reads as $a_{ps} = 27.2$ for linear chains as well as for stars with up to at least 12 arms [21]. Bearing in mind that in the MC systems $u = 0$ is already attained by less attractive interaction potentials between polymer segments for small chains, less repulsive parameters $a_{ps} < 27.2$ between polymer beads and solvent beads should suffice for $u = 0$ in case of DPD simulations. Actually, a value $a_{ps} = 27.0$ seems appropriate for the range of arm length evaluated, see inset of Fig. 4.

4.2. Shielding factors

Shielding factors K_{ce} for the contact formation between the center of the star and the end of the linear chain based on Monte Carlo simulations are shown in Fig. 5, those based on dissipative particle dynamics in Fig. 6. In each case the upper diagram depicts K_{ce} as functions of chain length m (with $m = 9$–257 MC segments and $m = 2$–32 DPD beads, respectively) for both athermal (full circles), and theta conditions (open circles). For MC + EE simulations an intermediate endothermal case is shown in addition (crossed circles) as well as results obtained by use of energy parameters slightly above (−0.255) and below (−0.27) the theta value (−0.261) thus giving limits for a theta region (broken lines).

Looking first at the K values of athermal systems both MC and DPD curves sharply drop with increasing chain length in the short chain length regime and show only small changes at (comparably) longer chain lengths. Although being restricted to a smaller range of chain lengths DPD results fully agree with those obtained by MC + EE.

Focusing on the theta curves (open circles) one can clearly see that these are similar in shape (compared to athermal conditions) but shifted to significant higher K-values. Again the decrease of K values is more pronounced in the regime of short chain lengths and than levels off for longer chains.

At first glance this behavior is quite an amazing one: in spite of a larger segment density (polymer coils under theta conditions are less expanded then in athermal solvent) the contact probability is increased. Admittedly, the actual (unweighted) number of accepted pairs with certain segments in contact – as evaluated in the MC + EE approach – is the smaller the worse the solvent quality simulated. However, an, e.g., center-end contact indirectly gives rise to further contacts resulting in a large Boltzmann factor of those configurations and accordingly to large K-values due to the weighting procedure. Thus, in the theta regime each polymer molecule serves as good 'solvent' for the other polymer and therefore configurations with more segments in contact are favored including the specific contacts evaluated.

In the DPD simulations the same behavior is found although – contrary to the MC + EE approach – the orientation of coils evolves dynamically and no weighting procedure is adopted! Due to the bad solvent condition polymer beads of some coil are effectively 'drawn' into another one as soon as they come into contact giving rise to smaller shielding as compared to athermal solvent conditions.

Thus, results of MC + EE obtained by proper weighting of pair configurations are fully supported by a second method (DPD) which is based on a completely different approach.

Calculations for other solvent conditions in between athermal and theta have been restricted to MC + EE. All curves are similar in shape and are located between the limiting cases. As an example the curve for $\varphi = -0.150$ (crossed circles) is shown in Fig. 5.

For a closer investigation of the dependence on chain length log–log plots of K_{ce} vs. m are shown in the lower diagram of Fig. 5 (MC + EE data) and Fig. 6 (DPD data), respectively, for the same conditions discussed above. For a specific solvent quality all points are fairly well located on straight lines (which result from linear regressions) and thus allow to express the dependence of shielding factors K on chain length m by scaling laws $K = A \cdot m^{\varepsilon}$, with ε directly given by the slope of the line and the prefactor calculated by use of the intercept.

For athermal conditions $\varepsilon \approx -0.47$ (−0.48) obtained by MC + EE (DPD) and for theta conditions the exponent reads as $\varepsilon \approx -0.16$ (−0.17). Prefactors A are 0.85 (0.87) for the former and 1.25 (1.05) for the latter. Again, results of MC + EE and DPD fairly well coincide and for both simulation methods K values are not only larger for theta conditions as compared to athermal ones but in addition are showing a much smaller chain-length dependence.

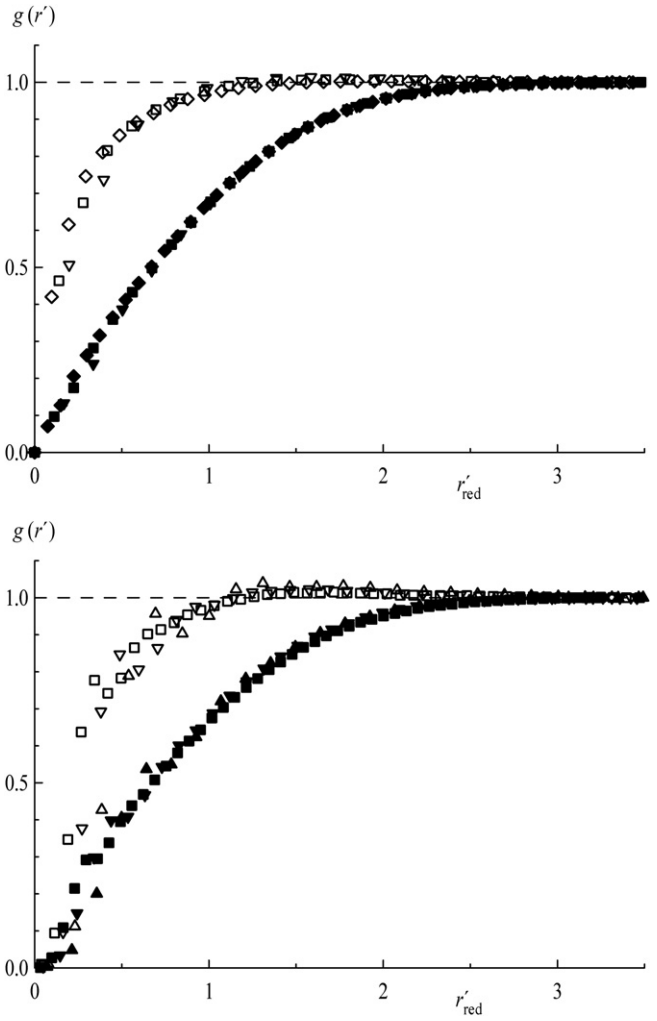

Fig. 9. MC (top) and DPD (bottom) center-end distribution function vs. the reduced separation distance between the center of the star and the end of the linear chain. Symbols as in Figs. 3 and 4, respectively.

Equivalent log–log plots of K values for a large number of energy parameters between athermal and theta conditions are also located on straight lines with slopes between the values reported above (not shown apart from $\varphi = -0.150$). Exponents and prefactors are summarized in the first set of columns of Table 1. Closer inspection reveals a smooth dependence of both the prefactors and the exponents on the energy parameter. While ε steadily decreases with increasing solvent quality (starting from theta conditions) and exhibits values between −0.10 at $\varphi = -0.27$ and −0.47 for $\varphi = 0$ the prefactor A first increases from $A = 1.12$ ($\varphi = -0.27$) to a maximum of $A \approx 1.34$ around $\varphi \approx -0.21$ and then decreases to $A = 0.85$ at athermal conditions.

Even though we are mainly interested in the central step of Z-RAFT star polymerization and thus in the shielding of reactions between the star center and the end of linear chains we computed two further cases for comparison (as already mentioned above). The second set of columns of Table 1 shows prefactors and exponents for the contact formation between a segment located at the middle of an arm of the star and the terminal segment of the linear chain (K_{me}) while the third set of columns gives A and ε for contacts between the end segments of the arms as well as of the linear chain (K_{ee}).

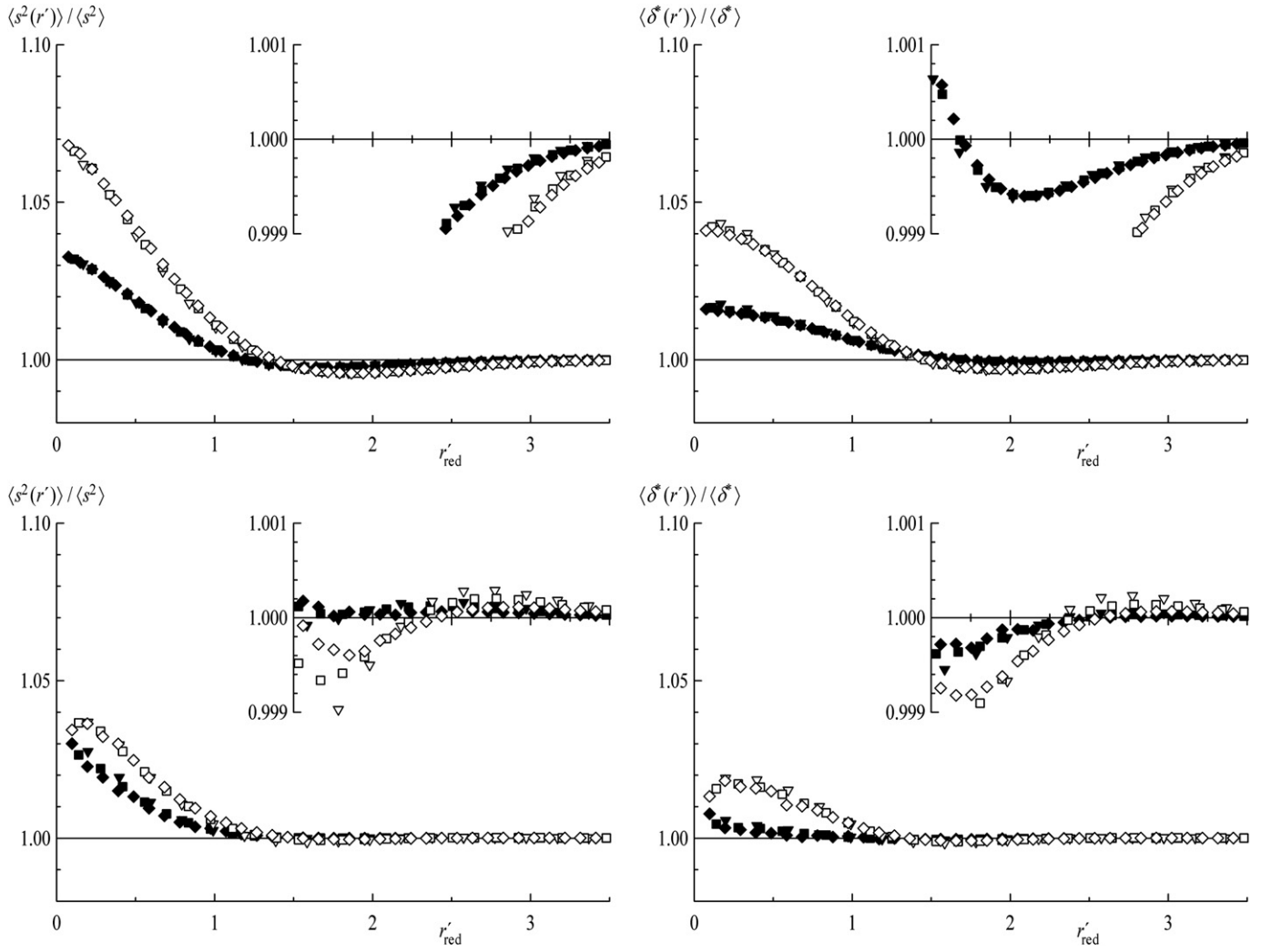

Fig. 10. MC + EE size and shape characteristics (analogous to Fig. 7), however, as functions of the reduced center-end distance. Symbols as in Fig. 7.

For all energy parameters evaluated $\varepsilon_{ce} < \varepsilon_{me} < \varepsilon_{ee}$ (e.g., $-0.47 < -0.29 < -0.16$, $-0.17 < -0.10 < -0.05$, and $-0.16 < -0.09 < -0.04$ for $\varphi = 0$, -0.255 and -0.261) indicating an increase of the chain-length dependence with decreasing distance of star segments from the center.

It is interesting to note that ε_{me} compares well to ε_{ce} of two linear chains (of same length), i.e., case "b1" reported in [24], $\varepsilon = -0.285$ and -0.11 for $\varphi = 0$ and -0.255. Similarly, ε_{ee} values for end–end reactions between linear chains (-0.155 and -0.065 for $\varphi = 0$ and -0.255) are nearly the same, the correspondence again being better for $\varphi = 0$. Thus, as long as the locations of segments of an arm are far from the center of the star, the situation is similar to an isolated chain at least for the chain-length dependence of shielding.

It should be mentioned that the present MC + EE data calculated for athermal conditions also compare well to our former results [13,14] where scaling laws were based on the number of bonds n instead of the number of segments m.

4.3. Position dependent properties

Prior to reactions between active sites polymer chains are forced to penetrate each other. The probability of close contacts between linear chains is rather large, especially in bad solvent, due to well-known mechanisms in order to minimize the volume of overlap [31]. The behavior of the pair distribution function of the present unsymmetrical situation has been already discussed in Section 4.1 and rather good compatibility of configurations in close contact was found also for these systems. Analogously to the symmetric case, it is expected that both the linear chains as well as the star-branched molecules have to undergo some characteristic changes in size and shape to reach such high compatibilities even at small separation distances. To depict this behavior the relative deviation of the mean square radius of gyration and the asphericity parameter from its respective value at infinite separation is plotted as function of separation distance in Figs. 7 and 8 for MC and DPD calculations, respectively. In each case the upper left plot shows $\langle s^2(r)\rangle/\langle s^2\rangle$ of the linear chain (open symbols) and the star (full symbols) for different chain lengths vs. the reduced separation distance r_{red} between their centers of gravity in case of athermal conditions. Starting from infinite separation the mean square dimensions of the two molecules decrease – the chains compress each other – with decreasing distance causing both the star and the linear chain taking slightly more symmetric shapes (which is depicted in the upper right plots, showing the deviation of the asphericity parameters). To demonstrate these effects conveniently the inset in each plot shows a scale-up of the region of first interaction. At

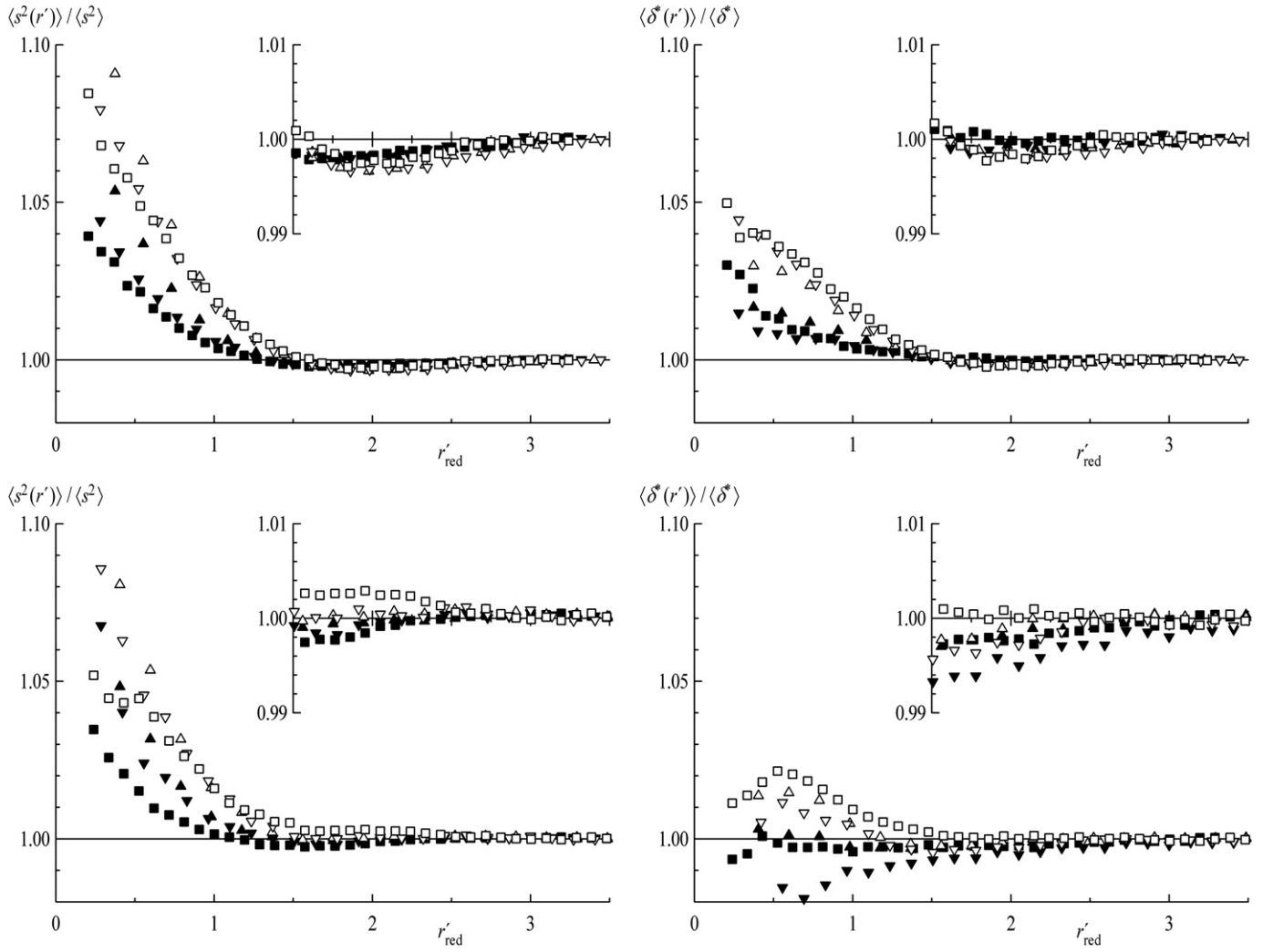

Fig. 11. DPD size and shape characteristics (analogous to Fig. 8), however, as functions of the reduced center-end distance. Symbols as in Fig. 8.

a certain distance $r_{red} \approx 1.5$ for the star and $r_{red} \approx 1.1$ in case of the linear chain, when both molecules start to penetrate each other, they appreciably increase in size, the relative effect being smaller for the star. Concomitantly the two molecules get first more asymmetric, however – contrary to the linear chain – the star-branched molecule reaches a more symmetric configuration at zero separation than at infinite distance.

At pseudo-ideal solvent conditions (pictured in the lower diagrams of Figs. 7 and 8) the situation is slightly different. The general behavior indeed is the same, however, looking at the region of first interactions (again scaled-up in the respective insets) quite the contrary trend can be observed. This is due to the attractive interactions between the two molecules forcing them to increase in size in the beginning of their approach.

Prior to reaction not only (unselective) penetration of molecules discussed above is necessary but in addition an approach of reactive sites. Thus, with respect to Z-RAFT polymerization the distribution function $g(r')$ of the distance r' between the center of the star and the end segment(s) of the linear chain is of interest as well as size and shape of configurations as a function of r' above all for small separations. In Fig. 9 $g(r')$ is shown as a function of the reduced distance r'_{red} (i.e., distance in units of the root mean square radius of gyration of the star). For athermal conditions (full symbols) $g(r')$ steadily decreases with decreasing distances, finally reaching the value of 0 for $r'_{red} = 0$ which is due to an overlap of the two MC segments (and the point of maximum repulsion of the two DPD beads, respectively). Similar to $g(r)$, for theta conditions $g(r')$ is larger than for athermal ones and exceeds unity in a certain range of large distances – again providing negative and positive contributions to u which clearly is also accessible on the basis of $g(r')$.

It should be noted that due to the underlying cubic lattice model in case of MC + EE $g(r')$ approaches the value $(z/6)\,K_{ce}$ with $z = 6 - F$ (and $F = 4$ in the present study) at a distance of $r' = 1$ lattice unit between the center of the star and the end of a linear chain for both athermal and theta solvent conditions. Concerning DPD, the peak (shoulder) in $g(r')$ at $r' = 1$ clearly visible in the smoothed presentation, Fig. 1, is hard to detect but nevertheless existing in the reduced presentation, Fig. 9.

In Fig. 10 (MC + EE) and Fig. 11 (DPD) the variation of size and shape as a function of r'_{red} is shown. For small distances the star as well as the chain exhibit expanded configurations (i.e., are increased in size) the effect being larger for the linear chain, as not all arms of the star will be perturbed by the 'attacking' chain. Asphericity (especially in case of the linear chain) is increased too, both mechanisms reducing the volume of overlap between the (non-reactive) segments. Behavior of larger distances is in accordance with the findings of center of mass separations as discussed above.

4.4. Experimental results

In order to probe the unexpected theoretical prediction that the contact probability between terminal ends of arm polymer and star centers increases in poor solvents, we performed experimental Z-RAFT star polymerizations using a tetrafunctional RAFT agent **1** (see Scheme 1) leading to four-arm stars. The increased contact probability directly translates to an increased addition rate of macroradicals toward RAFT-groups. It was found in earlier kinetic simulation studies [33] that an increased addition rate in RAFT polymerization leads to increased molecular weight control, that is, to decreased polydispersity indices, PDI, values. Four-arm-star polymerizations were thus probed with respect to the PDI of the resulting polymer, both in the poor solvent cyclohexane as well as in the good solvent toluene. Polymerizations were performed at relatively low temperatures of 47 °C in order to be as close as possible to the theta-temperature of polystyrene in cyclohexane ($T_\Theta = 35$ °C). In addition, solvent concentrations were chosen to be as high as possible (3:1 solvent to monomer on volume base) in order to compensate for the good solvent properties of the monomer styrene.

Fig. 12 depicts two pairs of representative molecular weight distributions with almost identical peak molecular weights of four-arm polystyrene produced in cyclohexane and toluene, respectively. It is extremely gratifying to see that both distributions of star polymers produced in the poor solvent cyclohexane (dashed lines) are significantly narrower than the ones generated in the good solvent toluene (full line). That is, the PDI values are indeed smaller in the case of Z-RAFT star polymerization being performed in poor solvents, which is in full accordance to the theoretical predictions. This observation is true for all star-shaped polystyrene samples obtained with different RAFT agent concentrations, as seen in Fig. 13, in which PDI values for two series of Z-RAFT star polymerizations are shown as function of monomer conversion. (For further details regarding experimental features and data interpretation of Z-RAFT star polymerizations, the reader is referred to [34]). It can hence be concluded that the quality of molecular weight control can truly be enhanced when performing Z-RAFT star polymerizations in poor solvents.

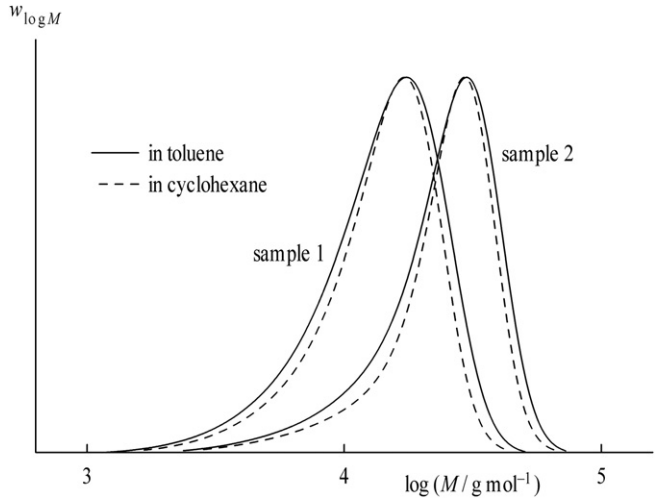

Fig. 12. Molecular weight distributions (SEC-curves), $w_{\log M}$, of exemplifying polystyrene samples produced in **1**-mediated solvent polymerization (3:1 solvent:styrene) at 47 °C using di(2-ethylhexyl)peroxycarbonate as initiator, *sample 1*: $t = 16$ h (20% monomer conversion) and *sample 2*: $t = 120$ h (50% monomer conversion). M is the apparent molecular weight from SEC calibration against linear standards [22].

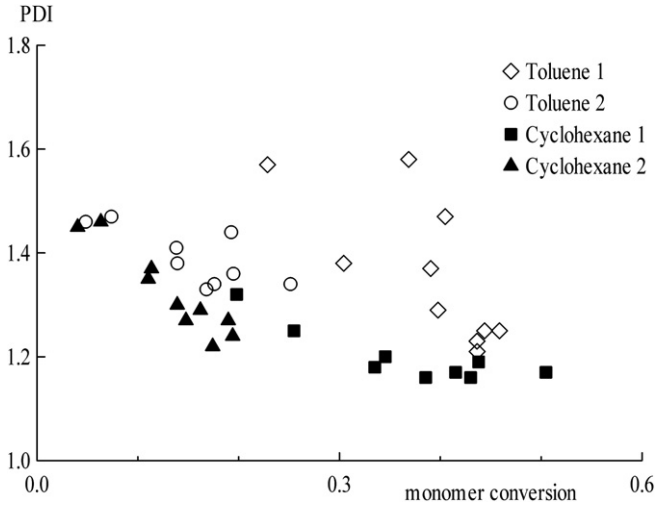

Fig. 13. Polydispersity index, PDI, vs. monomer conversion in **1**-mediated styrene Z-RAFT star polymerization at 47 °C in solution of toluene and cyclohexane (3:1 solvent to monomer), respectively. Series 1: $c_{RAFT} = 2.5$ mmol L^{-1} $c_{initiator} = 2.5$ mmol L^{-1}; series 2: $c_{RAFT} = 5$ mmol L^{-1} $c_{initiator} = 1.4$ mmol L^{-1}.

5. Conclusions

Comparable results have been obtained by use of two conceptually different methods, i.e., Monte Carlo simulations combined with exact enumeration on the one hand and a dynamic method – dissipative particle dynamics – on the other, thus verifying each other.

Shielding factors K for the contact formation between the center of star-branched molecules and the end of linear chains (mimicking the controlling reaction of Z-RAFT star polymerization) decrease with increasing chain lengths, however, were found to increase with decreasing thermodynamic solvent quality. The chain-length dependence of K – which can be described adequately by use of power laws – is significantly less pronounced in the regime of theta solvent conditions yielding an exponent of around −0.16 (which by chance is equivalent with findings for the athermal end–end contact probability of two linear chains) compared to athermal solvents for which K drops with an exponent of approximately −0.47. It can hence be concluded that the addition reaction in (four-arm) Z-RAFT star polymerization under theta conditions should be faster than the same one under good solvent conditions and that linear increase of molar mass with monomer conversion should be ensured up to higher degrees of polymerization due to the smaller chain-length dependence of shielding. This prediction has been confirmed experimentally by the finding that the polydispersity of Z-RAFT star polymer decreases when the solvent quality is decreased.

Acknowledgements

We are grateful for funding from the Austrian Science Fund FWF (P20124). Parts of these calculations were performed on the *Schrödinger Linux Cluster* and the *Vienna Scientific Cluster* which is gratefully acknowledged. Financial support by the *Deutsche Forschungsgemeinschaft* (VA226/3-2) is gratefully acknowledged. P.V. acknowledges receipt of a Heisenberg-Professorship (DFG).

References

[1] Graessley WW, Roovers J. Macromolecules 1979;12:959.
[2] Grest GS, Fetters LJ, Huang JS, Richter D. Adv Chem Phys 1996;94:67.
[3] Hirao A, Hayashi M, Tokuda Y, Haraguchi N, Higashihara T, Ryu SW. Polym J 2002;34:633.
[4] Hirao A, Inoue K, Higashihara T. Macromol Symp 2006;240:31.

[5] Chiefari J, Chong YK, Ercole F, Krstina J, Jeffery J, Le TPT, et al. Macromolecules 1998;31:5559.
[6] Barner-Kowollik C, Davis TP, Heuts JPA, Stenzel MH, Vana P, Whittaker M. J Polym Sci A Polym Chem 2003;41:365.
[7] Moad G, Rizzardo E, Thang SH. Aust J Chem 2005;58:379.
[8] Matyjaszewski K, Davis PT. Handbook of radical polymerization. New York: Wiley; 2002.
[9] Boschmann D, Vana P. Polym Bull 2005;53:231.
[10] Boschmann D, Vana P. Macromolecules 2007;40:2683.
[11] Stenzel MH, Davis TP. J Polym Sci A Polym Chem 2002;40:4498.
[12] Boschmann D, Manz M, Poppler AC, Sorensen N, Vana P. J Polym Sci A Polym Chem 2008;46:7280.
[13] Fröhlich MG, Vana P, Zifferer G. Macromol Theory Simul 2007;16:610.
[14] Fröhlich MG, Vana P, Zifferer G. J Chem Phys 2007;127:164906.
[15] Hoogerbrugge PJ, Koelman JMVA. Europhys Lett 1992;19:155.
[16] Groot RD, Warren PB. J Chem Phys 1997;107:4423.
[17] Lal M. Mol Phys 1969;17:57.
[18] Madras N, Sokal AD. J Stat Phys 1988;50:109.
[19] Metropolis N, Rosenbluth AW, Rosenbluth MN, Teller AH, Teller E. J Chem Phys 1953;21:1087.
[20] Zifferer G. Macromol Theory Simul 2000;9:479.
[21] Nardai MM, Zifferer G. J Chem Phys 2009;131:124903.
[22] Boschmann D, Edam R, Schoenmakers PJ, Vana P. Polymer 2008;49:5199.
[23] Mayadunne RTA, Jeffery J, Moad G, Rizzardo E. Macromolecules 2003;36:1505.
[24] Olaj OF, Zifferer G. Makromol Chem 1988;189:1097.
[25] Horie K, Mita I, Kambe H. Polym J 1973;4:341.
[26] Solc K. J Chem Phys 1971;55:335.
[27] Solc K, Stockmayer WH. J Chem Phys 1971;54:2756.
[28] Aronovitz JA, Nelson DR. J Phys (Paris) 1986;47:1445.
[29] Rudnick J, Gaspari G. J. Phys A Math Gen 1986;19:L191.
[30] Zifferer G. Macromol Theory Simul 1999;8:433.
[31] Olaj OF, Lantschbauer W, Pelinka KH. Macromolecules 1980;13:299.
[32] Vogel T, Bachmann M, Janke W. Phys Rev E 2007;76:061803.
[33] Vana P, Davis TP, Barner-Kowollik C. Macromol Theory Simul 2002;11:823.
[34] Boschmann D, Mänz M, Fröhlich MG, Zifferer G, Vana P. ACS Symp Ser 2009;1024:217.